Desalination 615 (2025) 119224

Contents lists available at ScienceDirect

Desalination

journal homepage: www.elsevier.com/locate/desal

Single-pass forward osmosis for efficient feed concentration: Optimizing multiple modules arrangement and flow distribution

Rajashree Yalamanchili, Pere Olives Cegarra, Albert Galizia, Ignasi Rodriguez-Roda, Gaëtan Blandin *

LEQUIA, Institute of Environment, University of Girona, 17003, Spain

HIGHLIGHTS

- FO pilot study on series and tree arrangements in single-pass operation.
- MATLAB-based mass transfer model experimentally validated in both flow orientations.
- Enhanced performance of counter-current flow evident with high-osmotic-pressure FS.
- Series and co-current tree arrangements were limited by unbalanced flow rates.
- Counter-current tree ensured balanced flow, achieving FS concentration factor 5.1.

GRAPHICAL ABSTRACT

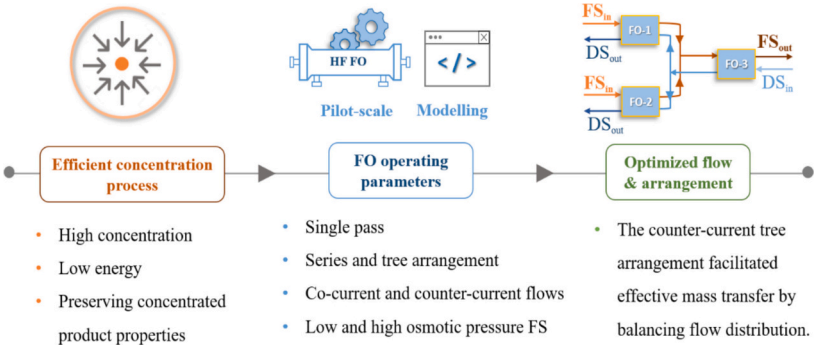

ARTICLE INFO

Keywords:
Concentration process
Counter-current flow
Forward osmosis
Module arrangement
Modeling
Single-pass

ABSTRACT

Forward osmosis (FO) is gaining prominence as a concentration process. However, most systematic studies remain limited to setups involving recirculating feed solution (FS) and draw solution (DS), and employing small membrane coupons or single module, thereby limiting insights into high-recovery concentration performance at the system scale. Realizing the full potential of FO for concentration purposes and maximizing osmotic energy efficiency requires a detailed understanding of module arrangements, flow dynamics, and their influence on operational scalability. This study presents pilot-scale investigation of FO modular arrangements, including series and tree configurations operated in single-pass mode under both co-current and counter-current flow orientations, combined with MATLAB-based mass transfer modeling. Experiments used Aquaporin HFFO2 hollow fiber (HF) modules and tested both low-osmotic-pressure (DI water) and high-osmotic-pressure (5 g/L saline) FS. The model showed strong agreement with experimental results and enabled detailed evaluation of spatial performance variations, enhancing evaluation of system scalability and efficiency. The full potential of counter-current flow emerged in multi-module setups. With a 5 g/L FS, series and tree arrangements initially performed similarly, achieving FS concentration factors of 4.59 and 5.10, respectively. Simulations revealed that water permeation in the series arrangement progressively diluted the DS, increasing its volumetric flow and leading to hydraulic imbalances that limit the system's ability to handle long-term stable operation. The tree arrangement faced similar challenges under co-current flow, but counter-current operation mitigated them by ensuring balanced flow distribution across stages, sustaining stable flux (4.76–6.71 LMH) and achieving an

* Corresponding author.
E-mail address: gaetan.blandin@udg.edu (G. Blandin).

https://doi.org/10.1016/j.desal.2025.119224
Received 23 April 2025; Received in revised form 17 July 2025; Accepted 20 July 2025
Available online 23 July 2025

overall recovery of 80.40 %. To further enhance the system performance, the impact of hydraulic conditions was explored through simulations to identify operating regimes with optimal trade-offs.

1. Introduction

Concentration processes are widely used across industries to separate water or solvents and isolate valuable compounds. They support key applications in chemical manufacturing, biotechnology, food processing, and environmental management [1–3]. Conventional concentration methods, such as thermal and membrane-based processes, have long been the backbone of industries like desalination, wastewater treatment, food processing, and pharmaceuticals. Thermal methods, such as evaporation, effectively remove solvents but have significant drawbacks, including high energy consumption and potential degradation of heat-sensitive compounds [4,5]. Pressure-driven membrane processes, including reverse osmosis, micro-filtration, and ultra-filtration, offer more energy-efficient alternatives but struggle with fouling, scaling, and limited performance with high-concentration feeds, often requiring extensive pre-treatment [6,7]. These limitations highlight the need for energy-efficient approaches that maximize concentration while preserving product integrity.

Forward osmosis (FO) is an innovative membrane technology that has gained significant attention as a separation process. Using a concentrated draw solution (DS), FO pulls water through a semi-permeable membrane from a feed solution (FS), driven solely by the osmotic pressure difference between the two solutions [8]. Unlike pressure-driven processes, FO can harness osmotic energy from existing saline sources such as seawater, brine, or industrial streams. FO membrane offers major advantages including low fouling nature [9], ease of cleaning [10] and a high rejection rate of broad range of contaminants [11,12]. Additionally, energy consumption in FO is limited to circulating FS and DS solutions, making it a low-energy alternative for concentration processes [13]. With its broad applicability, FO is increasingly considered in diverse sectors, including water treatment, wastewater recovery [14,15], integrated desalination and water reuse [16,17], and food processing [18,19]. Its effectiveness in concentrating and separating valuable compounds positions FO as a transformative solution for industries seeking efficient technologies.

Achieving high recovery rates in concentration processes is crucial for maximizing resource utilization, minimizing waste, and reducing operational costs across industries. In FO systems, recovery performance is governed by operating parameters such as membrane module design, module arrangement, flow orientation, and process conditions [20–23]. Despite FO's potential, most optimization-focused FO studies have been confined to single-module experiments with recirculating FS and DS, as summarized in Table 1. Even pilot-scale studies targeting applications like wastewater volume reduction have typically employed single FO modules with membrane areas between 0.3 and 0.5 sqm under recirculation mode [24–26]. While such configurations enable membrane performance evaluation, they lead to progressive dilution of the DS and mixing of concentrated FS with incoming FS, thereby reducing the osmotic pressure gradient and compromising the driving force for water flux. Other studies have also sought to optimize FO performance. Sanahuja-Embuena et al. reported that operating conditions and draw solute concentration significantly influence performance due to internal concentration polarization (ICP) [27]. Similarly Im et al. investigated FO modules for hybrid FO- reverse osmosis (RO) integration, emphasizing the role of DS concentration and flow rates on the performance of spiral-wound (SW) and flat-sheet elements [28].

Additionally, bench-scale experiments focusing on FO optimization are confined to small-scale membrane coupons [21,29–32]. While effective for membrane performance testing, these setups are limited when the objective is to evaluate system-level concentration capacity. In parallel, modeling and simulation approaches have been extensively employed to advance the mechanistic understanding of FO processes and support system design [33–38]. For instance, Ali et al. developed a MATLAB-based graphical user interface to simulate full-scale FO systems using SW modules, providing a valuable tool for performance prediction [39]. Deshmukh et al. quantified the impact of ICP on flux limitations using a module-scale model [37], while Phuntsho et al. explored flow orientation effects in FO modules, showing the superiority of counter-current operation in maintaining flux [22]. Similarly, Kim et al. conducted a simulation-based evaluation of FO modular configurations in a FO-RO hybrid system for osmotic dilution, using empirical data from single-element experiments. They identified pressure buildup as a key constraint on the scalability of SW modules and proposed a two-stage parallel housing design to mitigate this limitation [20]. While these studies offer scientific guidance to membrane behavior and operating trade-offs, they offer limited exploration of efficient concentration of FS under high-recovery conditions.

While recent studies have advanced the application of FO and FO–RO hybrid systems for concentration, key limitations remain regarding optimized module arrangement, flow configuration in single-pass operation, factors critical for system-level optimization and scalability. For instance, Hao et al. investigated a four-step FO process that achieved a threefold concentration of a high-osmotic acrylamide solution. However, the setup was limited by the use of small-area membrane coupons (0.00385 m^2), operation in recirculation mode, and the continuous intake of fresh DS at each step [40]. Chen et al. implemented a FO–RO hybrid system using 12 FO modules arranged as three stages in series, each consisting of four modules operated in parallel. While the system achieved up to 90 % water recovery and identified FO–RO as a promising strategy for RO concentrate minimization in coal chemical wastewater treatment, the rationale behind the specific module configuration was not discussed, and no assessment was made regarding its optimality [41]. Im et al. applied a data-driven approach to analyze element-scale FO–RO hybrid systems, proposing multi-element configurations using spiral-wound (SW) and plate-and-frame (PNF) FO elements arranged in series [42]. However, no evaluation was made regarding alternative flow strategies and module arrangement in single-pass operation.

Despite extensive efforts, key gaps remain in optimizing FO module arrangements for efficient concentration toward upscaling, especially to explore the full capacity of single-pass configurations. Advancing FO's applicability in such settings and supporting practical scale-up requires a detailed understanding of how module arrangements and flow orientation impact system-level dynamics and performance. These design implications, however, remain underexplored, underscoring the need for experimental validation under realistic operating conditions.

To the best of our knowledge, this is the first pilot-scale FO study to evaluate multi-module arrangements in a fully single-pass operation, specifically targeting system-level concentration efficiency. This work addresses critical gaps in the current literature, where most experimental studies have focused on small-scale, single-module setups operated under recirculation, conditions that dilute the DS, reduce the osmotic driving force, and do not reflect scalable operation. In contrast, our study provides the following distinctive aspects:

- Evaluation of multiple FO modules (Aquaporin HFFO2) in single-pass mode, eliminating recirculation and preserving inlet FS and DS concentrations throughout the process.
- Comparative assessment of series and tree (two-stage FO) module configurations, to investigate how layout design affects system-level concentration performance.

Table 1
Overview of FO performance optimization studies: System configurations and investigated performance factors.

Type of study	FO Module configuration/ material/ manufacturer	Area (sqm)	No. of membrane elements employed (Single/ Multiple)	FS and DS flow (recirculation/one-pass)	Flow direction (s) tested	Key drivers of FO performance studied	Reference
Pilot-scale	SW8040/CTA/HTI and SW8040/ TFC/ Toray	9 (HTI) and 15 (Toray)	Single	Recirculation	co-current	Evaluated hydrodynamics, water and salt flux, FS pressure sensitivity to fouling, and effectiveness of osmotic/physical cleaning strategies	[43]
Pilot-scale	HFFO14/TFC/ Aquaporin	13.8	Single	FS: Recirculation; DS: with and without recirculation	counter-current	Evaluated water recovery, ammonium losses, pH impact, membrane rejection, continuous vs batch mode, and energy efficiency under high salinity DS	[44]
Pilot-scale	HFFO220/TFC/ Aquaporin	2.3	Single	Recirculation (solute-specific rejection tests), one-pass (FO module)	co-current and counter-current	Effect of DS type/concentration, flow rates, trans membrane pressure, and temperature on flux/ rejection; emphasized CP impact and solute-specific FO–RO rejection differences	[27]
Pilot-scale	FO 8040–85/CTA/ FTS	9.9	Multiple (12)	Recirculation	counter-current	Evaluated membrane-based reconcentration systems for minimizing RO concentrate volume in coal chemical wastewater treatment. The FO–RO hybrid system enabled 90 % water recovery, minimized fouling and reduced capital expenditure compared to alternatives.	[41]
Pilot-scale and simulation-based	SW8040/TFC/ Toray	15	Single	Recirculation	co-current with crossflow	Simulation of six FO modular configurations for seawater osmotic dilution; evaluated element limits per housing, FS/DS pressure balance, and benefits of PAO in multi-stage FO-RO systems	[20]
Pilot-scale and Modeling	SW/CTA/HTI	0.3	Single	Recirculation	co-current	Evaluated concentration factor for municipal wastewater, COD/ phosphorus rejection, ammonium/ nitrogen rejection, flux performance, fouling impact, and cake-enhanced concentration polarization effects during long-term FO operation	[26]
Pilot-scale	HPC3205/CTA/ Toyobo	31.5	Single	One-pass	counter-current	Evaluated FS and DS flowrates, temperature effects, FS recovery, water flux, reverse solute flux, long-term performance, and membrane permeability in the osmotic concentration process.	[45]
Pilot-scale and modeling	HPC3205/CTA/ Toyobo and HF/ TFC/Aromatec	31.5 (Toyobo) and 0.5 (Aromatec)	Single	One-pass: FS and DS (Toyobo), DS (Aromatec); Recirculation: FS (Aromatec)	counter-current	Evaluated membrane productivity, fouling potential, chemical cleaning efficiency, reverse solute flux, and organic solute passage	[46]
Experiment	SW/CTA/HTI	1	Single	Recirculation	co-current	Evaluated the impact of DS concentration on power density and water flux, explored FO–RO system design alternatives, and proposed four new FO module configurations to enhance water flux, backwashing efficiency, and reduce pressure drop	[47]
Experiment	CSM FO-4040/ TFC/ Torey and PFO-100/ -/Porifera	3.1 (Toray) and 7 (Porifera)	Multiple (5 SW and 4 PNF)	Recirculation	co-current	Element-scale FO–RO hybrid systems using SW and PNF modules (tested in series arrangement) showed that module number and arrangement strongly affect performance, with five SW or four PNF FO elements identified as optimal.	[42]
Experiment	N.A/TFC/ In house fabricated	0.003852	Single	Recirculation	co-current	A four step FO process was used to concentrate high-osmotic acrylamide solution from 200 to 600 g/L, with fresh DS applied at each stage.	[40]

(*continued on next page*)

Table 1 (*continued*)

Type of study	FO Module configuration/ material/ manufacturer	Area (sqm)	No. of membrane elements employed (Single/ Multiple)	FS and DS flow (recirculation/one-pass)	Flow direction (s) tested	Key drivers of FO performance studied	Reference
Lab-scale and element-scale experiments	SW/CTA/N.A and PNF/Polyamide/ N.A	Lab-scale: 0.002; Element-scale: 0.5 (SW) and 7 (flat sheet)	Single	Recirculation	Element-scale: co-current; Lab-scale: counter-current	Impact of DS concentration, FS/DS flow rates, and module structure on water flux and scalability for FO–RO integration	[28]
Experimental and modeling	SW 2521FO-MS/ HTI/ and PNF PFO 20/TFC/ Porifera	0.5 (SW) and 1 (PNF)	Single	Recirculation	counter-current	Evaluated the impact of cross flow velocities, DS concentration, and FS pressure on pressure drop, membrane displacement, and flux decline	[48]
Simulation and experimental validation	HF/CTA/Toyobo	31.5	Single	One-pass	co-current	Impact of DS and FS inlet concentration and flow rate on water flux, energy efficiency and required no. of single-element parallel modules to reach targeted dilution was analyzed	[23]
Modeling and module-scale experiment	SW8040/N.A/ Toray	15.3	Single	Recirculation	co-current	Impact of trans-membrane pressure, DS channel height, and hydrodynamic factors on water flux and concentration polarization	[49]
Experiment	SW8040/ TFC/ Torey and PNF/ TFC/ Porifera	15.3 (SW) and 7 (PNF)	Single	One-pass	co-current (SW) crossflow (PNF)	Impact of module type, number of serially connected elements, draw channel pressure drop, flow rate, and footprint on feed pressure drop, draw pressure drop	[50]
Modeling	SW8040/N.A/N.A and HF/N.A/N.A	14.4	–	Recirculation	co-current	Impact of module-scale design, crossflow stream orientation, membrane baffling, channel dimensions, and multi-stage recharge configuration on wastewater utilization and energy recovery efficiency in hybrid FO-RO and RO-PRO systems was analyzed	[51]
Modeling	HF/N.A/N.A	40.4	–	One-pass	counter-current	Impact of structural parameters, crossflow velocity, and DS concentration on water flux, membrane area, and system optimization	[52]
Modeling and experimental validation	Flat sheet/ CTA/ HTI	0.002	Single	One-pass	co-current and counter-current	Impact of osmotic equilibrium, operating parameters, crossflow mode, water flux, FS recovery rate, and final DS dilution on FO process performance	[22]
Modeling	SW8040/TFC/ Toray	N. A	–	One-pass	cross flow	Impact of draw solution inlet flowrate, number of elements in the pressure vessel, recovery rate, final DS concentration, and FS flowrate on system performance optimization was analyzed	[39]
Pilot scale and modeling	HFFO2/TFC/ Aquaporin	2.3	Multiple (3)	One-pass	co-current and counter-current	Impact of multiple module arrangements (series and tree), flow orientation and hydrodynamics on efficient FS concentration	This work

N.A – Not available; TFC – Thin-film composite; CTA – Cellulose triacetate; SW – Spiral wound; PNF – Plate and frame; HTI – Hydration Technology Innovations; FTS – Fluid Technology Solutions; RO – Reverse osmosis; PRO – Pressure retarded osmosis; HF – Hollow fiber.

- Testing under both co-current and counter-current flow orientations, to quantify the influence of flow direction on flux distribution and overall recovery.
- Coupling with MATLAB-based spatial modeling and simulation, to track key performance metrics along the membrane length and support system optimization.

These contributions provide experimentally validated strategies for improving recovery in high-strength applications, offering practical insights to guide the scalable and energy-efficient design of FO concentration systems. Building on these objectives, the investigation began with individual module testing under varied operating conditions, followed by system-level evaluation of series and tree configurations. These experiments were complemented by MATLAB-based modeling to analyze flow and performance dynamics under different operating conditions.

2. Methodology

2.1. Experimetal setup

In this pilot-scale study, three Aquaporin HFFO2 hollow fiber (HF) modules (designated FO-1, FO-2, and FO-3) were employed. Each module had an effective membrane area of 2.3 m^2. Supplied by

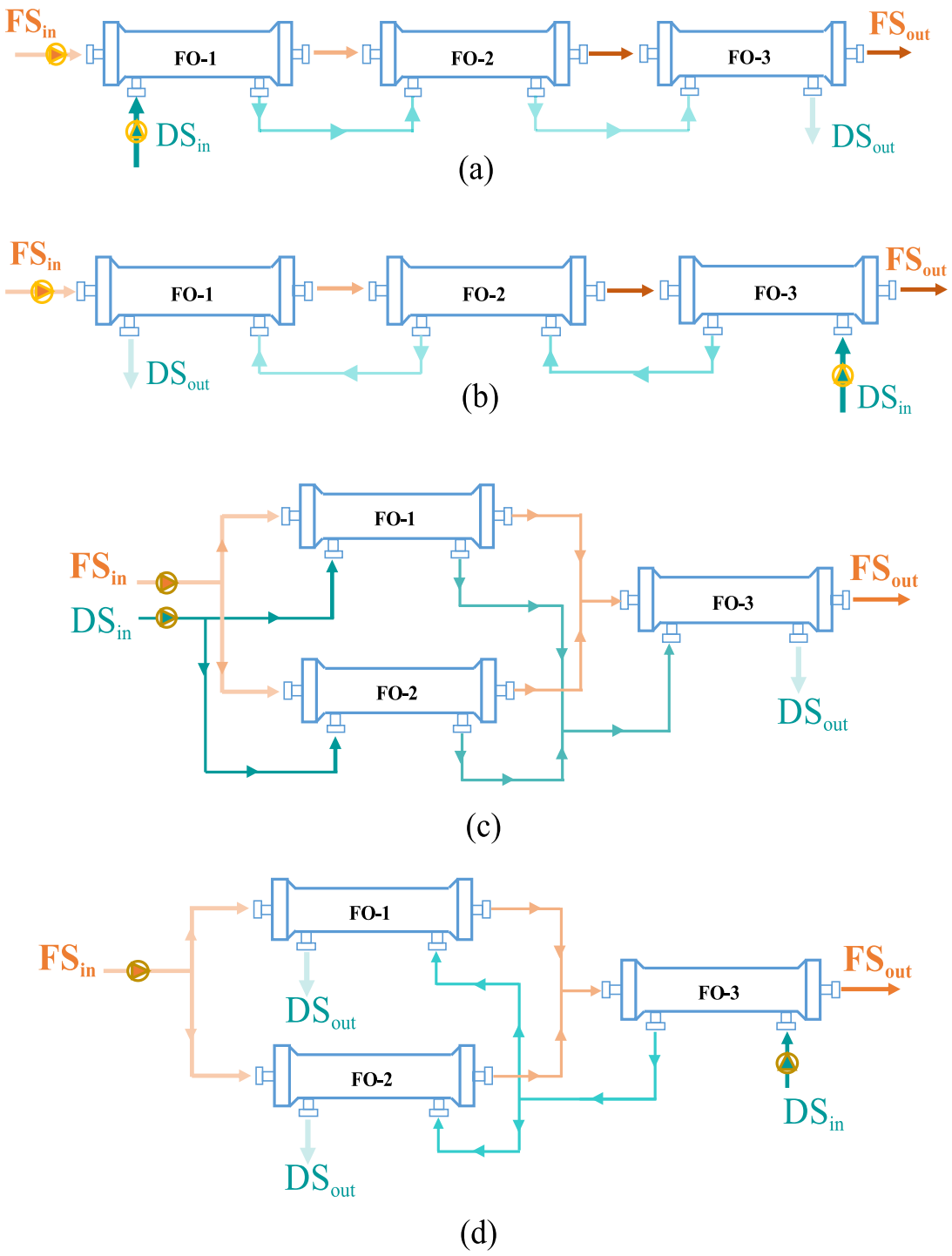

Fig. 1. FO module arrangements tested under single-pass operation: (a) Series co-current, (b) Series counter-current, (c) Tree co-current, and (d) Tree counter-current.

Aquaporin A/S (Lyngby, Denmark), these modules incorporate thin-film composite membranes featuring a polyamide selective layer embedded with aquaporin proteins, supported by a porous substrate. Each module measures 300 mm in length and 70 mm in diameter, with a negatively charged active layer [53]. The modules contain 30,800 fibers, each 270 mm long, with outer diameter of 0.27 mm [54]. The modules were stored at room temperature (~22 ± 1 °C) and thoroughly rinsed with deionized (DI) water before and after each experiment. All experiments were also conducted at room temperature to ensure consistency with storage and handling conditions. DI water used in the tests was produced from Milli-Q Progard TS2 module water system.

The initial phase focused on evaluating the performance of each module individually to identify any operational differences. Each of them was tested under two FSs: DI water and a 5 g/L saline solution, with a DS salinity of 35 g/L. All saline solutions were prepared using sea salt with a purity >99.4 % of sodium chloride (NaCl), supplied by Infosa (Barcelona, Spain). FS and DS inlet flow rate was set to 54 and 22.2 L/h respectively using Watson-Marlow Sci. 323 pumps (Watson-Marlow Flexicon A/S, Denmark). These flow rates were chosen to mimic the supplier's recommendations for optimal hydraulic conditions and

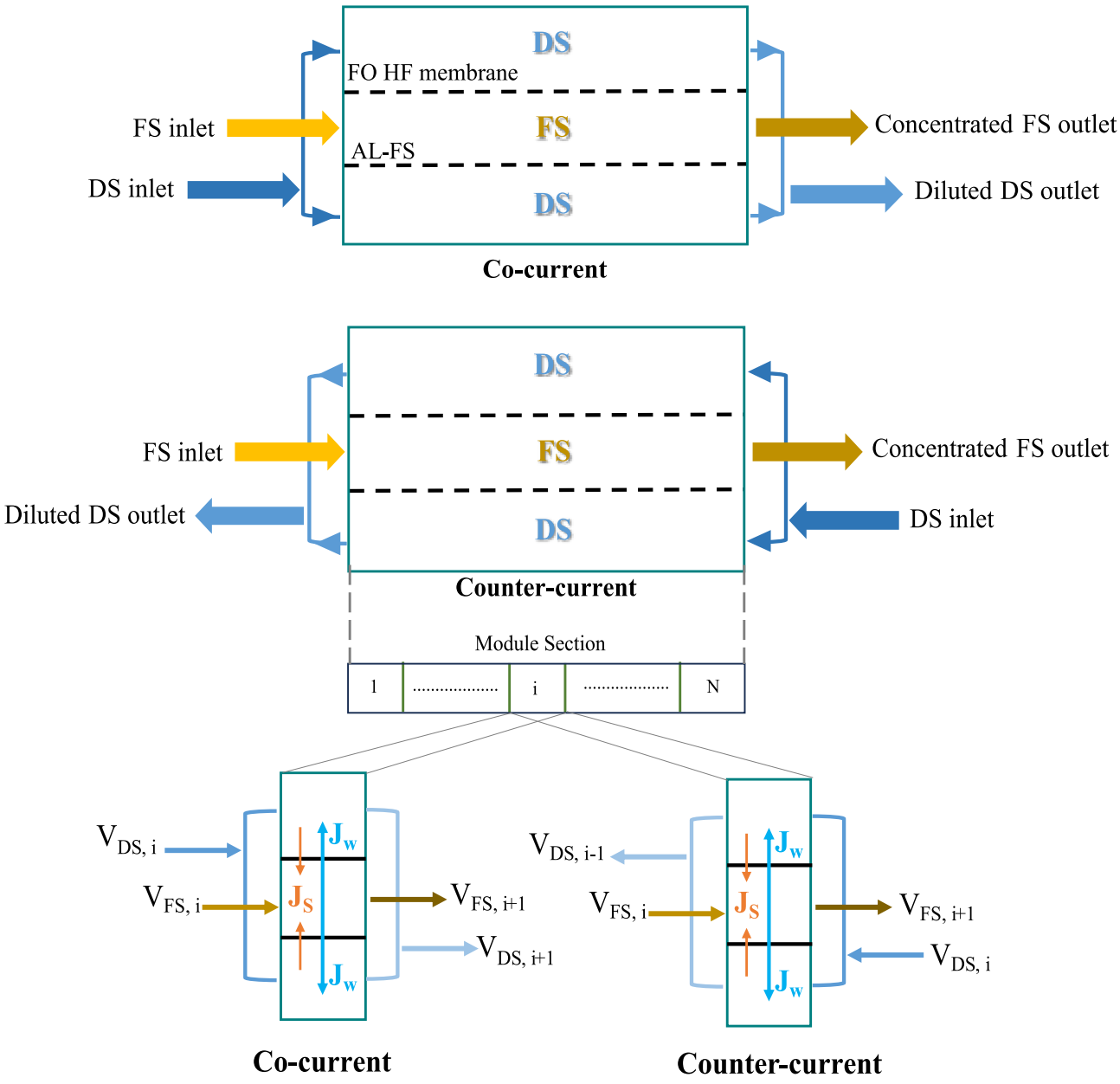

Fig. 2. Schematic representation mass transport in HF FO membrane in co-current and counter-current flow orientations considered in model simulations.

consistent membrane contact [53]. Both co-current and counter-current flow modes were tested to analyze the impact of flow orientation on key performance metrics, namely pure-water flux (J_w), FS recovery and concentration factor. The flow rates were determined using multiple Kern PCB 6000-1 balances (Balingen, Germany) placed under the FS inlet, FS outlet, and DS inlet to track mass changes over time. The difference between the FS inlet and outlet masses was used to calculate the permeate flow rate. The J_w was then calculated by dividing the volumetric permeate flow rate by the membrane surface area. In this study, FS recovery refers to volumetric water recovery from the FS, calculated as the percentage of feed water volume transferred to the DS during FO operation (Eq. (1)). The FS concentration factor represents the extent of feed concentration achieved and is calculated as the reciprocal of the remaining FS volume fraction (Eq. (2)).

$$\textit{FS recovery}\ (\%) = \frac{\textit{Volume of water permeated to DS side}}{\textit{initial FS volume}} \times 100 \qquad (1)$$

$$\text{FS concentration factor} = \frac{1}{1 - \text{FS recovery fraction}} \qquad (2)$$

In the later phase, maintaining the same inlet flow rates, two modules (FO-1+FO-2) were first connected in series, followed by the addition of a third module (FO-1+FO-2+FO-3). This setup enabled a detailed evaluation of FO performance and the impact of multi-module arrangements in both flow orientations. Fig. 1a and b illustrate the schematic representations of the series arrangement of FO modules in co-current and counter-current flow modes, respectively.

Finally, the tree arrangement was tested, with modules arranged in a branching pattern to enable parallel flows across two stages. In the co-current setup (Fig. 1c), the FS pump operated at 57 L/h, and the DS pump at 22.2 L/h, supplying both FO-1 and FO-2 modules. For the counter-current flow mode (Fig. 1d), the FS pump maintained the same flow rate of 57 L/h, serving FO-1 and FO-2, while the DS was introduced at FO-3 with an unchanged flow rate of 22.2 L/h, creating opposing flow directions across the stages.

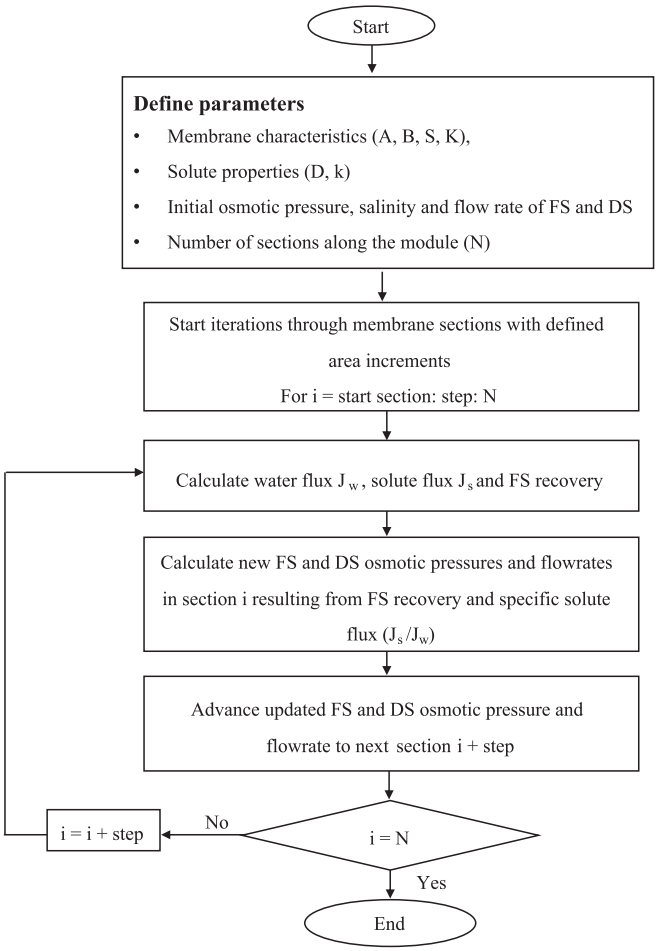

Fig. 3. Flowchart of the MATLAB-based modeling algorithm for simulating FO module performance. (a) Co-current and (b) Counter-current.

2.2. MATLAB-based model development

The efficiency of the FO process is inherently influenced by various mass transfer limitations, including ICP, external concentration polarization (ECP), and reverse solute diffusion (RSD). ICP occurs within the porous support layer of the FO membrane, where solute accumulation near the active layer reduces the effective osmotic pressure difference, thereby limiting water flux. ECP takes place outside the membrane surface, where solute buildup or depletion in the boundary layer near the FS or DS side further reduces the driving force for water transport. Unlike ICP, ECP can be alleviated by optimizing flow velocities and enhancing mixing. RSD, the backward diffusion of draw solutes into the FS, not only diminishes the osmotic driving force but also leads to contamination of the FS and increased operational costs due to the loss of draw solutes [55,56].

Both the FS and DS solutes are taken to be NaCl. The osmotic pressures in the FS and DS bulk solutions were approximated using the classical Van't Hoff equation, $\Pi = nCRT$ [22], where n is the Van't Hoff dissociation factor, (for NaCl, $n = 2$), C is the molar salt concentration, R is the universal gas constant, and T is the absolute temperature of the solution.

To account the impacts of ICP, ECP and RSD on the J_w, an advanced solution-diffusion model was employed for active layer facing FS, governed by a highly non-linear equation as described in previous studies [55,56] that captures the intricate interdependencies of this phenomena.

$$J_w = A.\left[\frac{\pi_{D\ bulk}.e^{-J_w \cdot K} - \pi_{F\ bulk}.e^{\frac{J_w}{k}}}{1 - \frac{B}{J_w}.\left(e^{-J_w \cdot K} - e^{\frac{J_w}{k}}\right)}\right] \tag{3}$$

In Eq. (3) J_w: water flux, A: membrane-specific pure water permeability, B: membrane-specific solute permeability, k: solute mass transfer coefficient, K: resistance to solute diffusion, π_{Dbulk}: osmotic pressure in bulk DS, π_{Fbulk}: osmotic pressure in bulk FS. The reverse solute flux (J_s) was calculated using Eq. (4) [55].

$$J_S = B.\left[\frac{C_{D\ bulk}.e^{-J_w \cdot K} - C_{F\ bulk}.e^{\frac{J_w}{k}}}{1 - \frac{B}{J_w}.\left(e^{-J_w \cdot K} - e^{\frac{J_w}{k}}\right)}\right] \tag{4}$$

In Eq. (4), $C_{D\ bulk}$: bulk DS concentration, $C_{F\ bulk}$: bulk FS concentration.

The key characteristics of the Aquaporin membrane employed in the modeling are: A of 1.56 LMH/bar, B of 6.67 $\times$ 10^{-8} m/s, structural parameter (S) of 0.15 mm [27]. The solute mass transfer coefficient (k) and bulk diffusion coefficient of the DS solute (D) are considered as 1.1 $\times$ 10^{-5} m/s and 1.47$\times$ 10^{-9} m^2/s respectively [56,57]. The resistance to solute diffusion (K) is calculated using Eq. (5) [56].

$$K = \frac{S}{D} \tag{5}$$

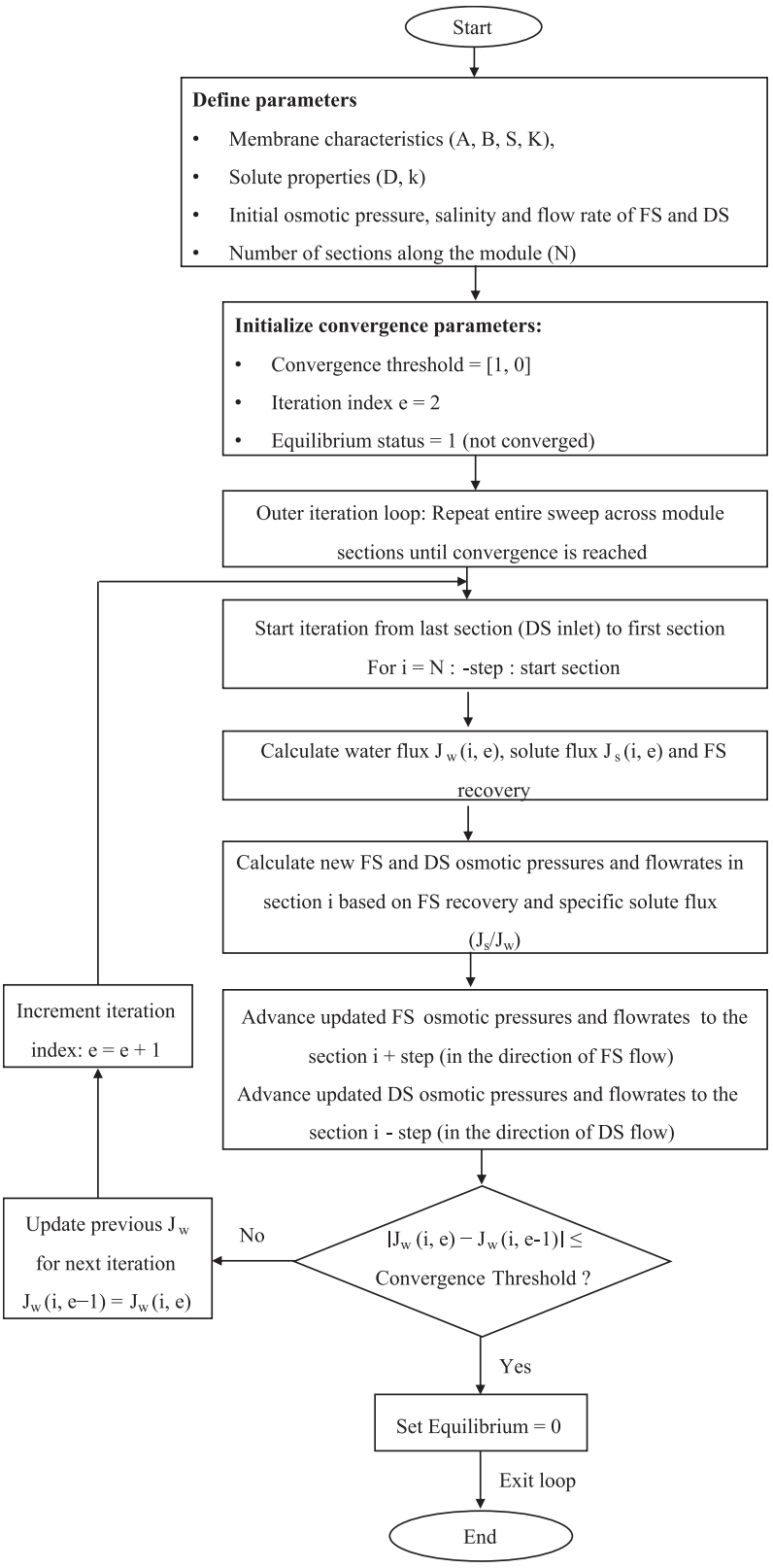

(b)

Fig. 3. (*continued*).

Fig. 2 depicts the schematic representation of mass transport within HF FO membranes for both co-current and counter-current flow modes as considered in the model simulations. The numerical simulation was solved iteratively. The module was sub-divided into N sections. The mass transfer coefficient was considered as constant along the length of the module. For the co-current flow mode, since both FS and DS enter

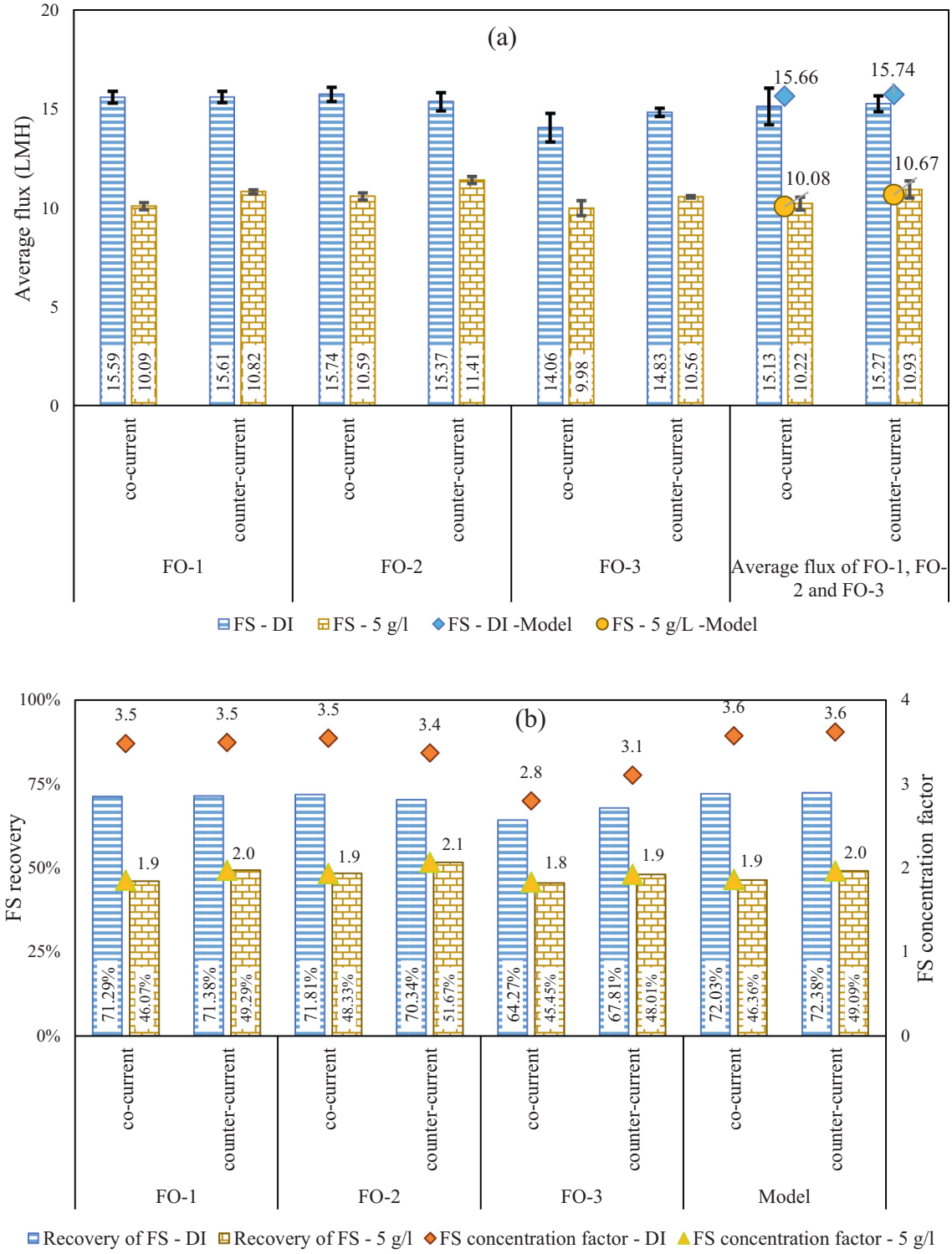

Fig. 4. Individual performance of FO modules, experimental and model results in different operating conditions. (a) Average flux and (b) FS recovery and concentration factor.

the module from same end the calculations were simple with their known bulk concentration. With each increase in membrane area, osmotic pressures and flow rates are updated based on the J_w and J_s/J_w from the previous section. The mass balance of FS and DS at each section in co-current were determined by Eqs. (6) and (7).

$$V_{FS,i+1} = V_{FS,i} - J_w A_i \quad (6)$$

$$V_{DS,i+1} = V_{DS,i} + J_w A_i \quad (7)$$

where V_{FS} and V_{DS} are volumetric flow rates of FS and DS respectively and A_i represents membrane area of sub-section. The subscript i indicates the current section, and i + 1 denotes the direction of flow progression to the next section in the co-current setup.

For counter-current flow, where the FS and DS enter from opposite

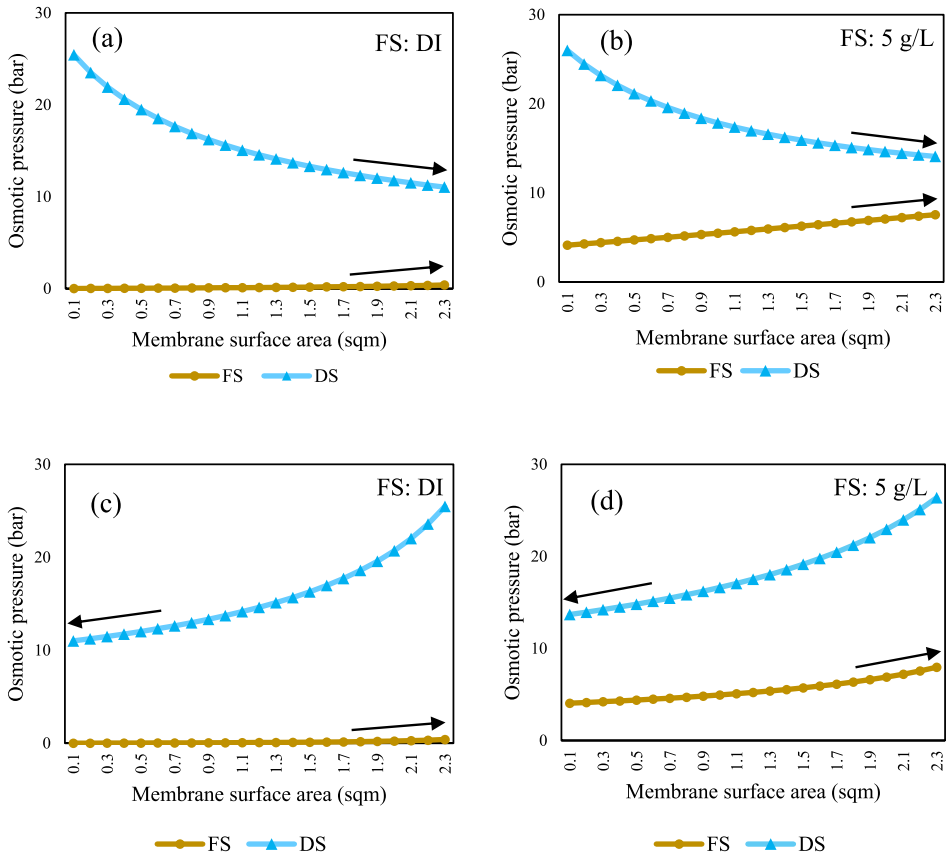

Fig. 5. Model projected osmotic pressure evolution across membrane surface for low and high osmotic pressure FS. Co-current: (a) DI Water, (b) 5 g/L; Counter-Current: (c) DI Water (d) 5 g/L.

ends of the module, the modeling process becomes more complex, as only one side (FS or DS) has a known inlet concentration and flow rate at each sub-section along the membrane. To address this, the current model assumes that the FS flows entirely through the module from its inlet, while the DS is introduced in reverse from the FS outlet end of the module (which is the DS inlet) toward the FS inlet [22]. Iterations were performed starting from sub-section N (where the DS enters) and proceed sequentially toward the beginning of the module. Within this setup, FS parameters (flow rate and osmotic pressure) are updated from sub-section i to i + 1, while DS parameters are updated from i to i – 1, reflecting their opposing flow directions. This indexing ensures that although both FS and DS are updated within the same loop index, they correspond to physically opposite directions along the module length. The mass balance for each sub-section is governed by Eqs. (8) and (9).

$$V_{FS,i+1} = V_{FS,i} - J_w A_i \quad (8)$$

$$V_{DS,i-1} = V_{DS,i} + J_w A_i \quad (9)$$

The modeling MATLAB-based algorithm for the FO module under co-current and counter-current flow direction is depicted in Fig. 3. The developed model was validated against experimental results, and key performance metrics were studied along the module length including flux, FS recovery, concentration factor, flow rates, and osmotic pressure evolution. Although fouling can inhibit efficient water transfer and increase the membrane area required, it does not affect the osmotic potential of FS and DS, which governs the osmotic equilibrium required to achieve high recovery. Therefore, fouling was not considered in the current model to simplify the analysis while focusing on key performance parameters.

3. Results

3.1.1. *Performance of individual FO modules and model validation*

As shown in Fig. 4, performance evaluation of individual modules (FO-1, FO-2 and FO-3) yielded highly consistent results, demonstrating the reliability of module performance under identical operation conditions. Performance variations were primarily influenced by FS composition (DI water vs. 5 g/L saline solution) rather than differences between modules. The model demonstrated strong agreement with experimental data, accurately predicting FO module performance for both DI water and 5 g/L FS under co-current and counter-current flow conditions.

While using DI water as the FS, all modules consistently achieved high fluxes, averaging 15.13 ± 0.93 LMH in co-current and 15.27 ± 0.40 LMH in counter-current flow modes (Fig. 4a). Recovery rates were similarly consistent, with an average of 69.12 ± 4.21 % in co-current and 69.84 ± 1.84 % in counter-current mode (Fig. 4b). The FS concentration factor stabilized between 3.1 and 3.5. This high flux is attributed to the strong osmotic gradient created by the absence of solutes in DI water, which drives water flow toward the 35 g/L NaCl DS. These minimal variations confirm the consistency of the module performance under identical conditions.

Consistent performance among modules was also observed with a 5 g/L saline FS (Fig. 4a), where average flux was 10.22 ± 0.32 LMH in co-current and 10.93 ± 0.43 LMH in counter-current flow modes. The decrease in flux was attributed to the lower initial osmotic pressure difference between the FS and DS compared to DI water as the FS. As a result, recovery rates declined to 46.62 ± 1.52 % in co-current and

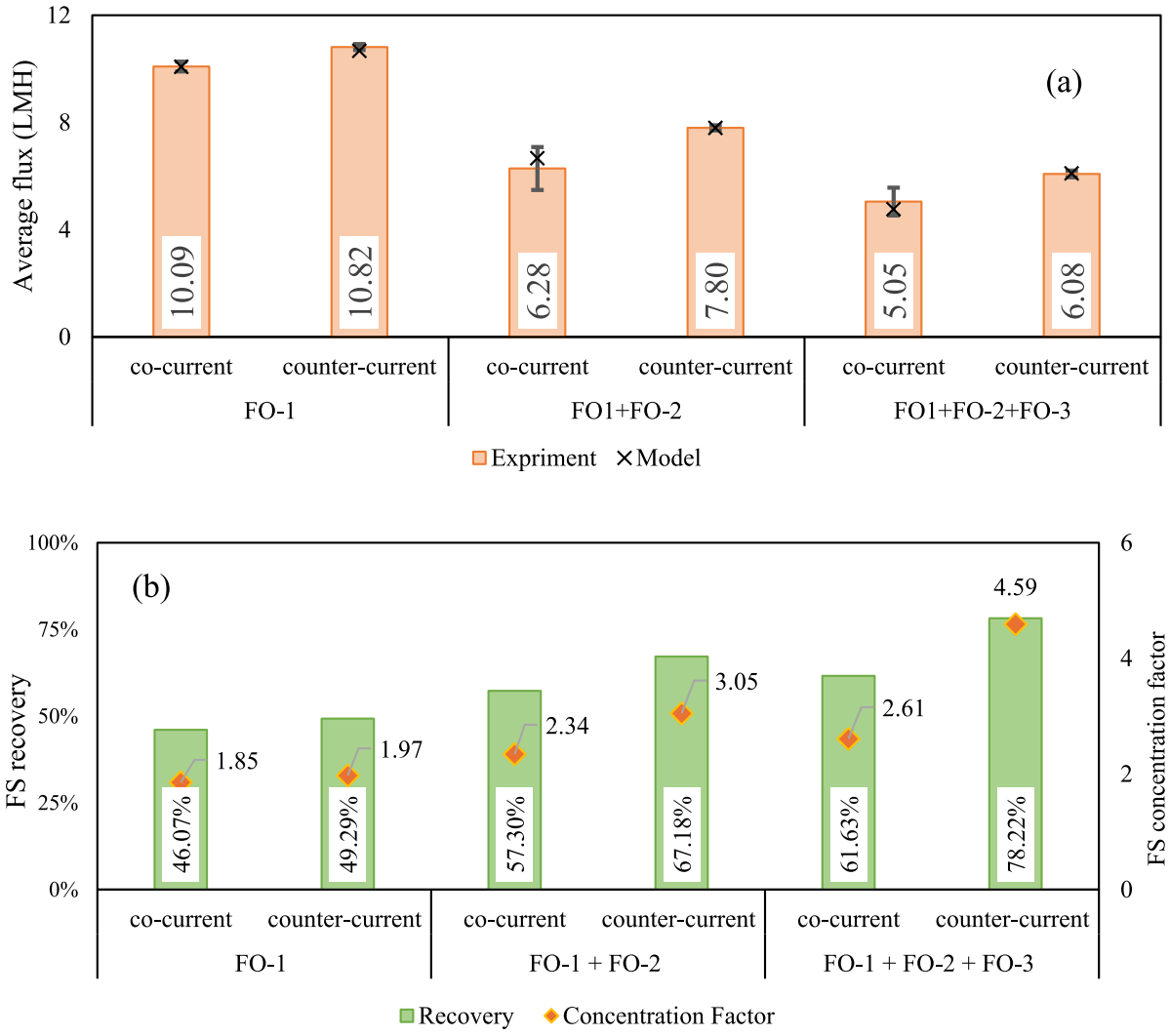

Fig. 6. Comparison of FO performance with 1, 2 and 3 modules in series with experimental results. (a) Average Flux, (b) FS recovery and concentration factor.

49.66 ± 1.86 % in counter-current mode, with the FS concentration factor reducing to 1.8–2.1 (Fig. 4b). These observations align with literature findings that highlight the critical role of FS salinity in FO performance, as higher FS salinity diminishes the osmotic potential and, consequently, the efficiency of the water transport process [21,30]. Building on these findings, no clear difference in performance was observed between co-current and counter-current flow orientations while operating in single module for both FS.

3.1.2. *Osmotic pressure evolution across membrane surface*

The model analyzed osmotic pressure distribution under varying conditions. For low osmotic pressure FS (DI), flow orientation had a negligible impact on the osmotic pressure gradient across the membrane (Fig. 5a and c). In co-current flow mode, the osmotic pressure difference tends to decline more sharply, particularly with high osmotic pressure FS (5 g/L), resulting in a steeper osmotic gradient across the membrane, as shown in Fig. 5b. Conversely, in counter-current flow mode, where the FS and DS move in opposite directions, the osmotic pressure difference is more evenly sustained across the module, as illustrated in Fig. 5d. Despite this advantage, the higher osmotic differential in counter-current flow did not translate into higher efficiency for single-module operation, leading to similar overall performance between the two flow orientations as observed earlier (Fig. 4).

3.2. *Series arrangement*

3.2.1. *Flux and recovery trends*

Fig. 6 presents the comparative performance of FO systems configured with one (FO-1), two (FO-1 + FO-2), and three (FO-1 + FO-2 + FO-3) modules in series. In all cases here, the FS and DS inlet flow rates were maintained at 54 L/h and 22.2 L/h, respectively. Initial trials with DI water as the FS established the system's potential to achieve complete recovery with 2 modules alone, where no water exits through FS outlet channel, which can lead to module damage. Thus, subsequent experiments were performed only under more challenging conditions, i.e., with a 5 g/L saline FS to better assess system performance under realistic conditions.

The addition of a second module led to a significant increase in FS recovery, improving by 11.23 % in co-current flow and 17.89 % in counter-current flow, compared to the single-module setup (Fig. 6b). However, this gain in recovery was accompanied by a flux reduction, with a 37.7 % decrease in co-current and 27.95 % decrease in counter-current flow modes (Fig. 6a). Introducing a third module further enhanced recovery, increasing by an additional 11.4 % in co-current flow and 10.5 % in counter-current flow, resulting in total recoveries of 61.63 % and 78.22 %, respectively (Fig. 6b). However, this improvement came at the cost of further flux reduction, with a 19.41 % drop in co-current flow and 14.83 % drop in counter-current flow, compared to the two-modules in series arrangement (Fig. 6a).

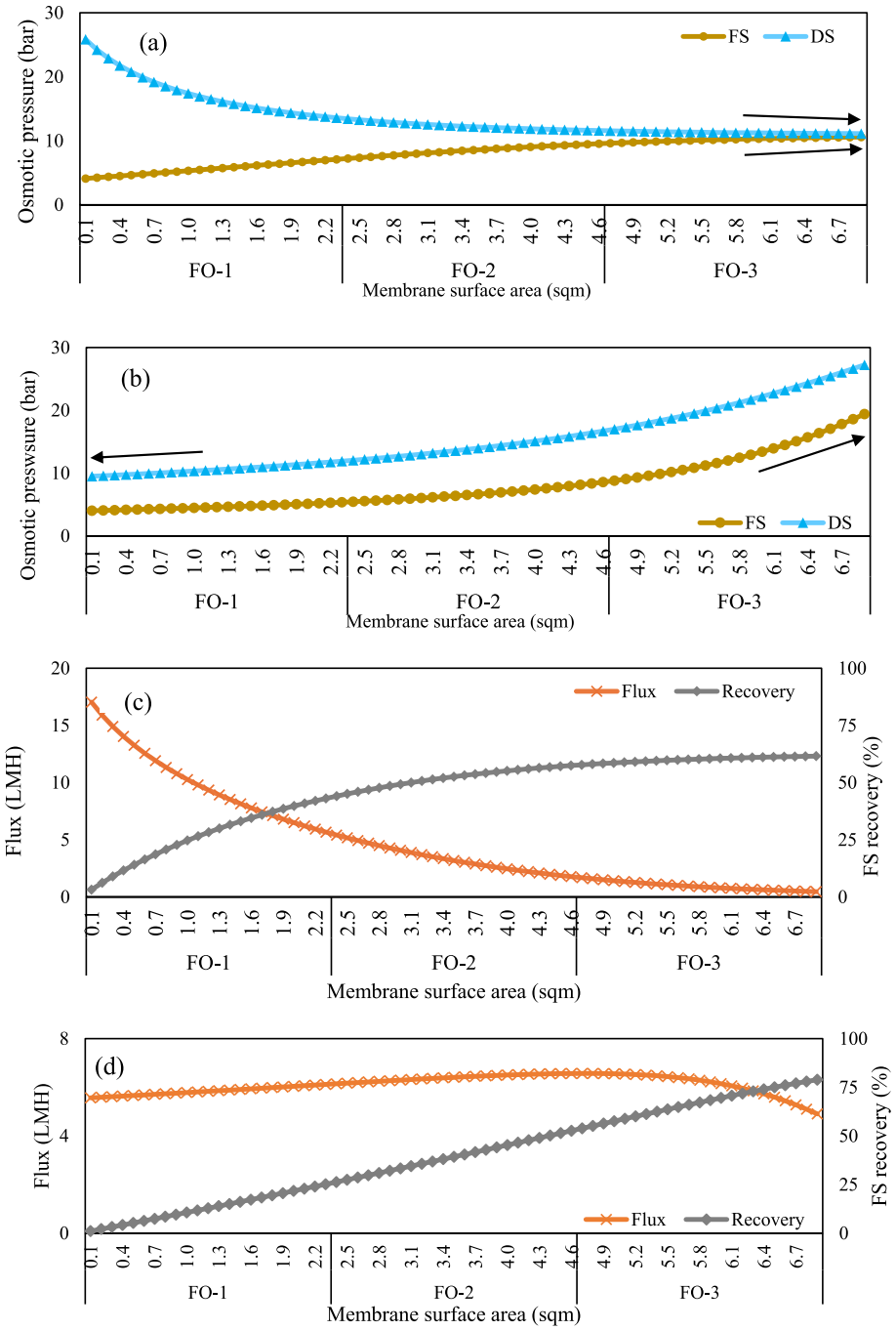

Fig. 7. Model projection of series arrangement performance. Osmotic pressure evolution: (a) Co-current and (b) Counter-current; Flux and FS recovery trends: (c) Co-current and (d) Counter-current.

These results highlight a trade-off in series operation: while additional modules improve recovery, they progressively reduce flux efficiency as the osmotic driving force declines [23]. With each module, FS concentration increases, lowering the osmotic pressure difference and limiting water transport, leading to diminishing flux. To counteract this decline, strategies that minimize osmotic gradient depletion while maintaining adequate driving force are essential. Optimizing module arrangements plays a key role in sustaining flux efficiency and maximizing overall recovery.

Notably, counter-current flow consistently outperformed co-current, especially as more modules were added. This advantage is attributed to better osmotic pressure distribution resulting from opposing FS and DS flow in the system. With two modules, counter-current flow achieved higher recovery than co-current flow even with three, as the latter experienced a more rapid decline in osmotic driving force, limiting further gains.

3.2.2. *Impact of flow orientation*

Modeling results revealed performance variations along the module length. In co-current flow, the osmotic pressure difference declined sharply along the modules, approaching equilibrium by the third module (Fig. 7a). The high initial osmotic gradient at the first module enabled a flux of 17.03 LMH, facilitating effective water transport and recovery. However, by the inlet of the third module, the flux had dropped to 1.68 LMH, further decreasing to 0.46 LMH at the outlet. This steep flux decline limited overall recovery to 61.57 % (Fig. 7c)

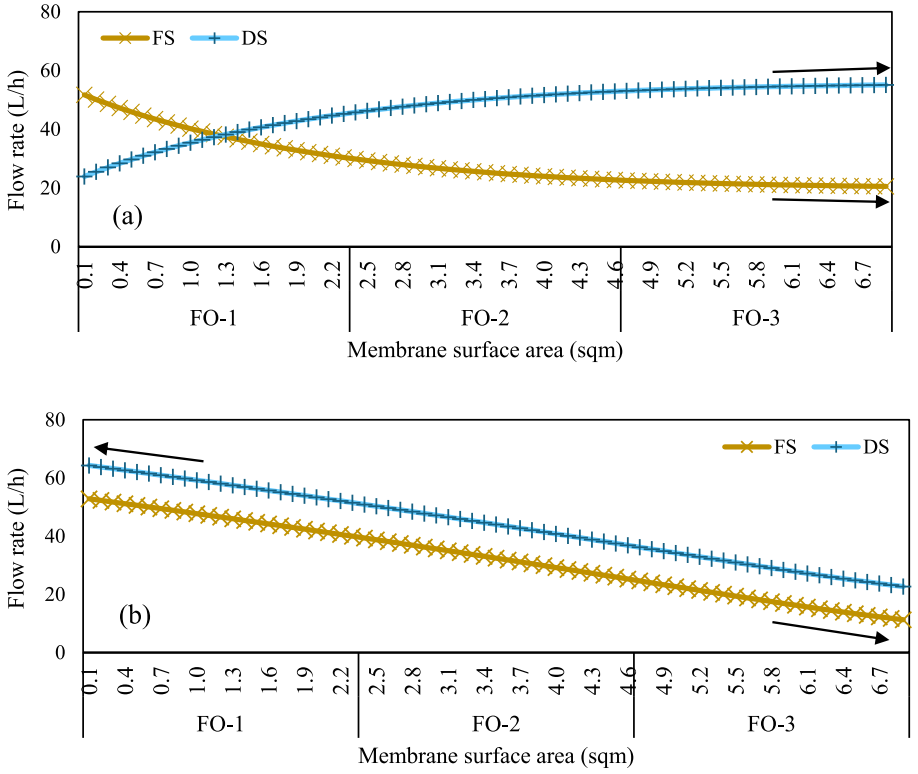

Fig. 8. Model-projected FS and DS flowrates in series arrangement with three modules. (a) Co-current and (b) Counter-current.

highlighting co-current flow's limitation in sustaining water extraction across modules. The rapid flux drop across modules not only restricts recovery efficiency but may also increase fouling risks and pressure instability, further constraining long-term performance [33,58].

In counter-current configuration (Fig. 7b), DS was introduced at the opposite end of the FS stream, maintaining a more balanced osmotic pressure gradient across the three-module train. This flow orientation sustained the driving force for water transport over the full membrane length, in contrast to the steep decline observed under co-current conditions (Fig. 7a). As a result, the system exhibited a relatively uniform flux profile, ranging from 4.9 to 6.5 LMH, and achieved an overall recovery of 78.88 % (Fig. 7d).

Although the initial flux was lower than in co-current mode due to the moderated osmotic gradient at the first module, the gradual decline in driving force led to more stable water transport and enhanced FS concentration in counter-current mode. Similar benefits of counter-current flow have been described in prior modeling studies [22,37] and single-module experiments [27]. This analysis quantifies the efficiency improvements across three modules in series, offering a more comprehensive understanding of its performance.

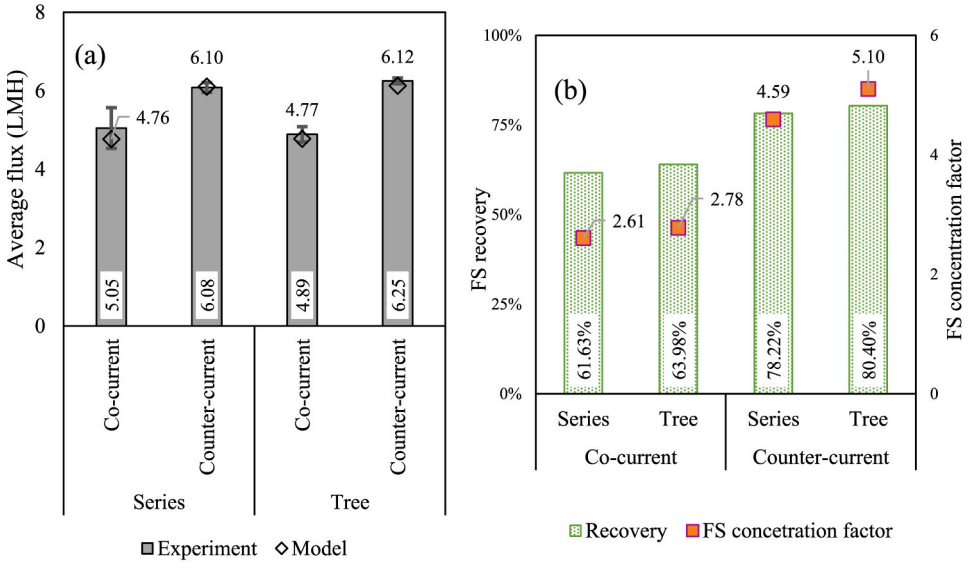

Fig. 9. FO performance in series and tree arrangements in both flow orientations. (a) Experimental and modeled average flux and (b) Experimental FS recovery and concentration factor.

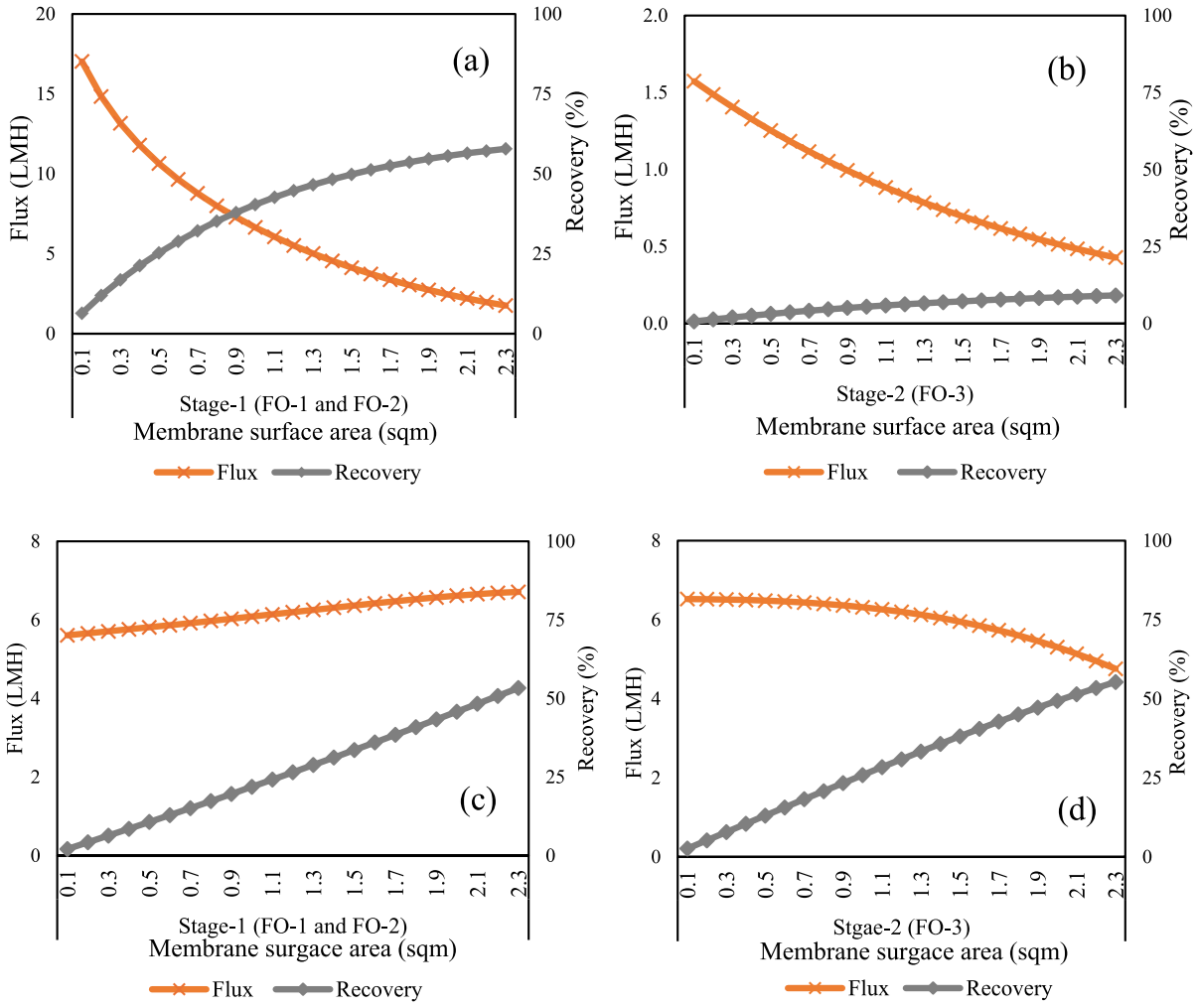

Fig. 10. Model projected flux and recovery trends DS in tree arrangements with two stages. Co-current: (a) Stage-1 and (b) Stage-2; Counter-current (c) Stage-1 and (d) Stage-2.

3.2.3. *Insights into flow dynamics*

Flow rate trends in co-current and counter-current modes offer insights into multi-module system scalability and stability. In the counter-current flow mode, the DS flow rate exhibited a steep increase from the first module to the last, with the final diluted DS flow volume reaching 64.32 L/h, 2.9 times the initial input (Fig. 8b). This substantial increase reflects the high flux potential of counter-current setups, which is critical for achieving superior FS concentration. However, the amplified flow rates can lead to hydraulic imbalances, potentially causing operational instability and exceeding recommended module specifications [53,59]. These challenges may impact long-term performance and scalability, while also straining system components and affecting durability.

In co-current flow, the diluted DS flow rate increased to 55.08 L/h, 2.3 times the initial input. (Fig. 8a). However, as observed in Section 3.2.2, the diminishing osmotic potential across the modules limited water transport efficiency, highlighting the constraints of co-current operation in multi-module series arrangements.

3.3. *Tree arrangement*

3.3.1. *Performance metrics from experiments*

Fig. 9a presents the average flux values for series and tree arrangements under both flow orientations, including both experimental and model results. Flux values were similar between series and tree configurations, with counter-current achieving higher flux compared to co-current. Consequently, counter-current flow resulted in higher FS concentration factors of 4.59 and 5.10 in series and tree configurations, respectively, while co-current was limited to 2.61 and 2.78 (Fig. 9b). Although experimental results indicated comparable overall performance between the two arrangements, they provided limited insight into spatial variations in key performance metrics, which were further evaluated through modeling to identify the most efficient concentration configuration. These aspects are systematically explored in Sections 3.3.2 and 3.3.3.

3.3.2. *Flux and FS recovery trends from model*

Fig. 10 presents the model-projected flux and recovery trends for the tree arrangement with two stages: Stage-1 (FO-1 and FO-2) and Stage-2 (FO-3), under both flow orientations. In co-current flow, flux peaked at 17.03 LMH in Stage-1 but rapidly declined to 1.76 LMH within the same stage, further dropping to 0.43 LMH in Stage-2. This sharp decline limited recovery to 57.82 % per module in Stage-1 and only 9.14 % in stage-2 (Fig. 10a and b), highlighting co-current flow's inability to sustain flux due to diminishing osmotic driving force.

In contrast, counter-current flow maintained more stable flux profiles, ranging from 5.61 to 6.71 LMH in Stage-1 and 4.76–6.52 LMH in Stage-2 (Fig. 10c and d). While initial flux was lower than in co-current, its stability resulted in higher recovery, reaching 53.31 % per module in Stage-1 and 55.30 % in Stage-2. This demonstrates counter-current flow's advantage in sustaining water transport efficiency and mitigating severe flux losses seen in co-current operation.

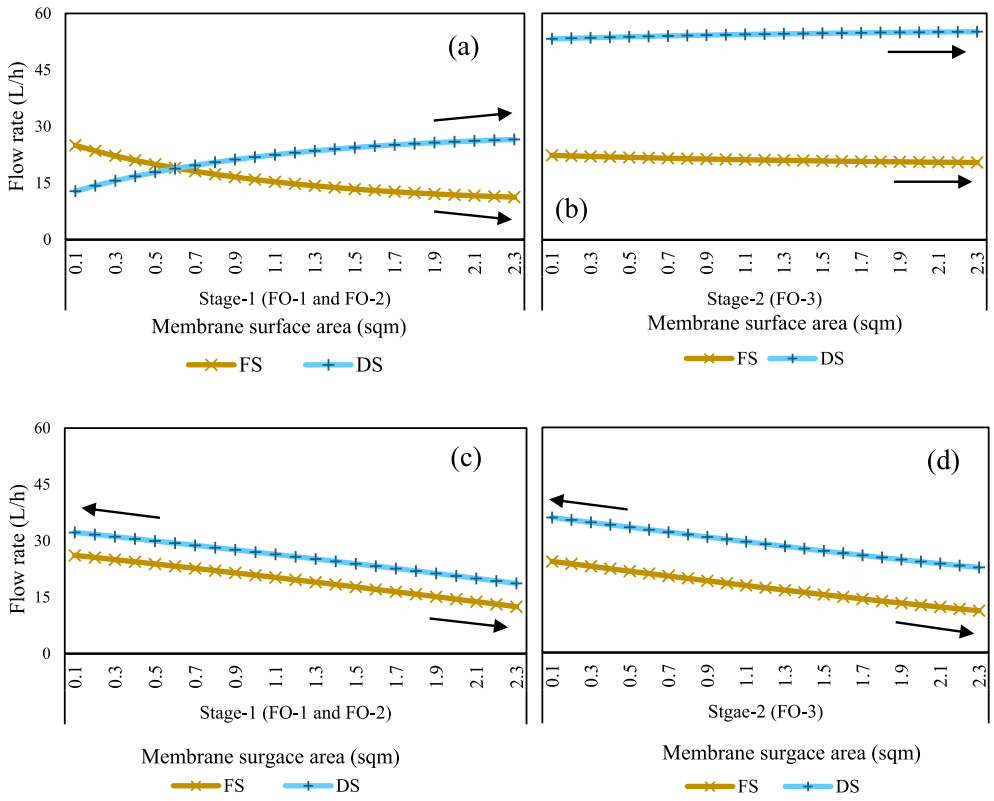

Fig. 11. Model-projected FS and DS flowrates in tree arrangement with two stages. Co-current: (a) Stage-1 and (b) Stage-2; Counter-current (c) Stage-1 and (d) Stage-2.

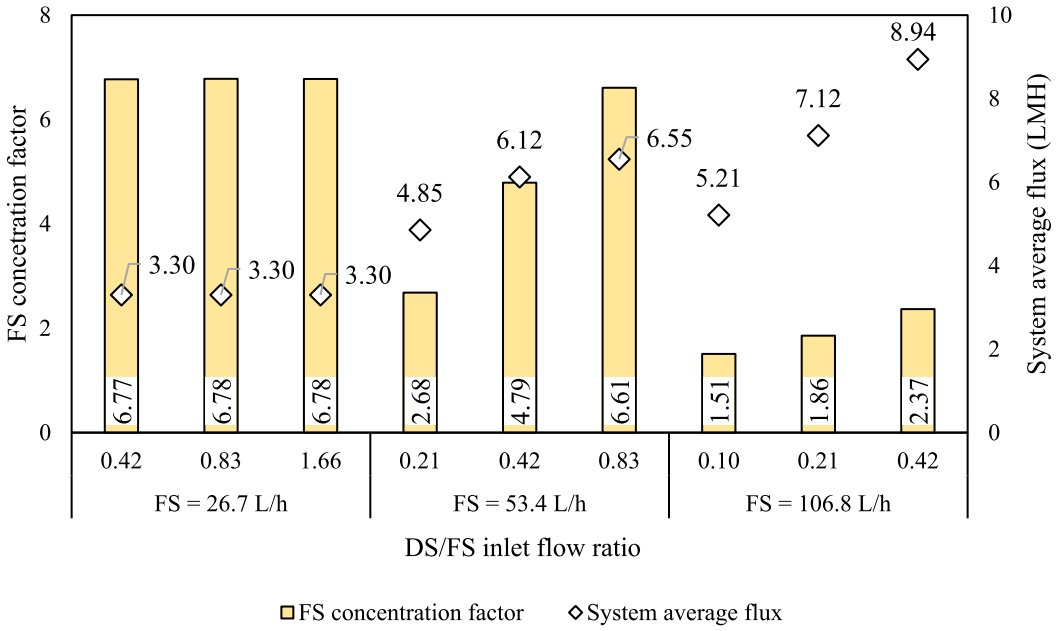

Fig. 12. Simulated impact of FS flow rate and DS/FS ratio on average flux and FS concentration factor under counter-current tree configuration.

3.3.3. Flow distribution across stages

In the co-current flow, the maximum recovery achieved in Stage-1 led to substantial dilution of the DS, increasing its volume to 53.24 L/h before entering Stage-2 (Fig. 11a and b). The total DS flow exiting the system was 2.5 times higher than the inlet volume. However, this increased dilution disrupted the hydraulic balance between FS and DS entering Stage-2, reducing osmotic pressure and limiting further water transport. Moreover, handling such high DS volumes could strain the module, potentially disrupting hydraulic stability and increasing the risk of fibers damage that could compromise system integrity.

The counter-current tree arrangement effectively mitigated the flow imbalances observed in other configurations. Despite achieving a high 55.3 % recovery in Stage-2, the diluted DS volume remained evenly distributed across Stage-1 modules, ensuring balanced flow throughout

the system (Fig. 11c and d). This structural advantage overcame the hydraulic instability seen in series and co-current tree arrangements, enabling higher overall recovery (80.40 % vs. 78.22 % in the series arrangement) while maintaining stable flux across both stages. Thus, the counter-current tree arrangement ensures hydraulic stability, offering an optimized configuration for efficient concentration process in single-pass.

3.4. Simulation-based analysis of hydraulic conditions influencing FO performance

To assess the influence of hydraulic conditions on system performance, the tree arrangement in counter-current flow was simulated under a range of FS flow rates and varying draw-to-feed (DS/FS) inlet flow ratios. Fig. 12 presents the simulated results, showing the effect of both FS flow rate and DS/FS ratio on average flux and FS concentration factor.

As FS flow rate increased, the FS concentration factor decreased, revealing an inverse relationship. For instance, at FS flow rate of 26.7 L/h, the system achieved a high FS concentration factor of ~6.7 despite operating at a relatively low average flux of ~3.3 LMH. As FS flow increased to 53.4 and 106.8 L/h, the average flux rose significantly, but the concentration factor declined. This trend can be explained by the fact that, at lower FS flow rates, the volume of feed per unit membrane area is smaller, allowing longer residence times and more complete water extraction. Although the flux is modest, the higher relative water recovery achieved under these conditions leads to greater FS concentration. Conversely, at higher FS flow rates, although flux rises, the shortened contact time resulted in lower recovery, which ultimately limited the concentration factor.

At a given FS flow rate, increasing the DS/FS inlet flow ratio generally enhanced both the FS concentration factor and the system average flux. This improvement is driven by the stronger and more sustained osmotic driving force created by the higher DS inflow, which facilitates greater water transport across the membrane.

However, an exception was observed at the lowest FS flow rate (26.7 L/h), where changes in DS/FS ratio had no impact. In this case, the average flux remained nearly constant (~3.3 LMH), and the concentration factor showed negligible variation. This is attributed to the inherently favorable mass transfer conditions at low FS throughput. Specifically, extended residence time and high membrane area-to-FS volume ratio which already enable efficient osmotic driving force utilization and high-water recovery. As a result, additional DS flow does not significantly improve performance under these conditions.

In contrast, at higher FS flow rates, increasing the DS/FS ratio had a pronounced effect. For instance, at an FS flow rate of 53.4 L/h, raising the DS/FS ratio from 0.21 to 0.83 increased the concentration factor from 2.68 to 6.61 and boosted the average flux from 4.85 to 6.55 LMH. Although higher DS flow requires greater draw consumption, it clearly enhanced final FS concentration.

Among the tested conditions, an FS flow rate of 53.4 L/h with a DS/FS ratio of 0.83 yielded the best trade-off between performance and hydraulic input achieving a high FS concentration factor of 6.61 and average flux 6.55 LMH offering practical insight for configuring FO systems targeting high single-pass concentration. While this condition delivers high FS concentration factor, it requires the highest DS flow input. This elevated DS consumption could pose a limitation, particularly in systems where the DS must be reconcentrated as it may lead to increased DS recovery costs.

4. Conclusion

Our findings provide a practical reference for optimizing FO module arrangement and flow distribution in single-pass concentration systems.

- A clear advantage of counter-current operation emerged when concentrating high-osmotic-pressure FS using multiple FO modules.
- In counter-current mode, while series arrangement achieved a FS concentration factor of 4.59, its scalability was limited by unbalanced hydraulic conditions. In contrast, the tree arrangement mitigated these limitations by distributing flow more evenly across modules, enabling it to reach a higher concentration factor of 5.1.
- Increasing the DS/FS ratio to 0.83 at 53.4 L/h FS flow enhanced the FS concentration factor to 6.61 in the tree configuration, highlighting the potential of hydraulic optimization, with associated trade-offs in flux behavior and DS demand.
- Future research could explore multi-stage tree arrangements to further enhance concentration efficiency. In addition, the development of a dedicated software tool that incorporates fouling dynamics and feedwater complexity could offer valuable guidance for design optimization and large-scale implementation.

CRediT authorship contribution statement

Rajashree Yalamanchili: Writing – review & editing, Writing – original draft, Visualization, Validation, Software, Methodology, Investigation, Formal analysis, Data curation. **Pere Olives Cegarra:** Writing – review & editing, Investigation, Formal analysis. **Albert Galizia:** Writing – review & editing, Software. **Ignasi Rodriguez-Roda:** Writing – review & editing, Supervision, Resources, Project administration, Funding acquisition. **Gaëtan Blandin:** Writing – review & editing, Writing – original draft, Supervision, Software, Resources, Methodology, Funding acquisition, Conceptualization.

Declaration of competing interest

The authors declare that they have no known competing financial interests or personal relationships that could have appeared to influence the work reported in this paper.

Acknowledgement

This work received the support of a fellowship from the “la Caixa” Foundation (ID 100010434). The fellowship code is LCF/BQ/PR21/11840009. Gaëtan Blandin acknowledges the Ramon y Cajal research fellowship RyC2022-035843-I funded by MICIU/AEI/10.13039/501100011033. LEQUIA [2021-SGR-01352] has been recognized as consolidated research group by the Catalan Government. Rajashree Yalamanchili was supported by a PhD grant from the University of Girona (IFUDG2022).

Open Access funding provided thanks to the CRUE-CSIC agreement with Elsevier.

Data availability

Data will be made available on request.

References

[1] G. Blandin, F. Ferrari, G. Lesage, P. Le-Clech, M. Héran, X. Martinez-Lladó, Forward osmosis as concentration process: review of opportunities and challenges, Membranes 10 (10) (2020) 284, https://doi.org/10.3390/membranes10100284.

[2] V. Sant’Anna, L.D.F. Marczak, I.C. Tessaro, Membrane concentration of liquid foods by forward osmosis: process and quality view, J. Food Eng. 111 (3) (2012) 483–489, https://doi.org/10.1016/j.jfoodeng.2012.01.032.

[3] L. Chekli, S. Phuntsho, H.K. Shon, S. Vigneswaran, J. Kandasamy, A. Chanan, A review of draw solutes in forward osmosis process and their use in modern applications, Desalination Water Treat. 43 (1–3) (2012) 167–184, https://doi.org/10.1080/19443994.2012.672168.

[4] A.A. Prestes, C.V. Helm, E.A. Esmerino, R. Silva, E.S. Prudencio, Conventional and alternative concentration processes in milk manufacturing: a comparative study on dairy properties, Food Sci. Technol. 42 (2022) e08822, https://doi.org/10.1590/fst.08822.

[5] J. Dumpler, T. Huppertz, U. Kulozik, Invited review: heat stability of milk and concentrated milk: past, present, and future research objectives, J. Dairy Sci. 103 (12) (2020) 10986–11007, https://doi.org/10.3168/jds.2020-18605.
[6] A. Alsobh, M.M. Zin, G. Vatai, S. Bánvölgyi, The application of membrane Technology in the Concentration and Purification of plant extracts: a review, Period. Polytech. Chem. Eng. 66 (3) (2022) 394–408, https://doi.org/10.3311/PPch.19487.
[7] C.Y. Tang, Y.-N. Kwon, J.O. Leckie, Fouling of reverse osmosis and Nanofiltration membranes by humic acid—effects of solution composition and hydrodynamic conditions, J. Membr. Sci. 290 (1–2) (2007) 86–94, https://doi.org/10.1016/j.memsci.2006.12.017.
[8] G. Blandin, A.R.D. Verliefde, J. Comas, I. Rodriguez-Roda, P. Le-Clech, Efficiently combining water reuse and desalination through forward osmosis—reverse osmosis (FO-RO) hybrids: a critical review, Membranes 6 (3) (2016) 37, https://doi.org/10.3390/membranes6030037.
[9] A. Achilli, T.Y. Cath, E.A. Marchand, A.E. Childress, The forward osmosis membrane bioreactor: a low fouling alternative to MBR processes, Desalination 239 (1–3) (2009) 10–21, https://doi.org/10.1016/j.desal.2008.02.022.
[10] B. Mi, M. Elimelech, Organic fouling of forward osmosis membranes: fouling reversibility and cleaning without chemical reagents, J. Membr. Sci. 348 (1–2) (2010) 337–345, https://doi.org/10.1016/j.memsci.2009.11.021.
[11] M. Salamanca, R. López-Serna, L. Palacio, A. Hernández, P. Prádanos, M. Peña, Study of the rejection of contaminants of emerging concern by a biomimetic aquaporin hollow Fiber forward osmosis membrane, J. Water Process Eng. 40 (2021) 101914, https://doi.org/10.1016/j.jwpe.2021.101914.
[12] G. Blandin, A.R.D. Verliefde, C.Y. Tang, A.E. Childress, P. Le-Clech, Validation of assisted forward osmosis (AFO) process: impact of hydraulic pressure, J. Membr. Sci. 447 (2013) 1–11, https://doi.org/10.1016/j.memsci.2013.06.002.
[13] W.Y. Chia, S.R. Chia, K.S. Khoo, K.W. Chew, P.L. Show, Sustainable membrane Technology for Resource Recovery from wastewater: forward osmosis and pressure retarded osmosis, J. Water Process Eng. 39 (2021) 101758, https://doi.org/10.1016/j.jwpe.2020.101758.
[14] T.Y. Cath, D. Adams, A.E. Childress, Membrane contactor processes for wastewater reclamation in space, J. Membr. Sci. 257 (1–2) (2005) 111–119, https://doi.org/10.1016/j.memsci.2004.07.039.
[15] G. Blandin, B. Rosselló, V.M. Monsalvo, P. Batlle-Vilanova, J.M. Viñas, F. Rogalla, J. Comas, Volatile fatty acids concentration in Real wastewater by forward osmosis, J. Membr. Sci. 575 (2019) 60–70, https://doi.org/10.1016/j.memsci.2019.01.006.
[16] V. Yangali-Quintanilla, Z. Li, R. Valladares, Q. Li, G. Amy, Indirect desalination of Red Sea water with forward osmosis and low pressure reverse osmosis for water reuse, Desalination 280 (1) (2011) 160–166, https://doi.org/10.1016/j.desal.2011.06.066.
[17] R. Yalamanchili, I. Rodriguez-Roda, A. Galizia, G. Blandin, Can a forward osmosis-reverse osmosis hybrid system achieve 90% wastewater recovery and desalination energy below 1 kWh/M3? A design and simulation study, Desalination 585 (2024) 117767, https://doi.org/10.1016/j.desal.2024.117767.
[18] E.M. Garcia-Castello, J.R. McCutcheon, Dewatering press liquor Derived from Orange production by forward osmosis, J. Membr. Sci. 372 (1–2) (2011) 97–101, https://doi.org/10.1016/j.memsci.2011.01.048.
[19] N.K. Rastogi, Applications of forward osmosis process in food processing and future implications, in: Current Trends and Future Developments on (Bio-) Membranes, Elsevier, 2020, pp. 113–138, https://doi.org/10.1016/B978-0-12-816777-9.00005-8.
[20] J.E. Kim, S. Phuntsho, S.M. Ali, J.Y. Choi, H.K. Shon, Forward osmosis membrane modular configurations for osmotic dilution of seawater by forward osmosis and reverse osmosis hybrid system, Water Res. 128 (2018) 183–192, https://doi.org/10.1016/j.watres.2017.10.042.
[21] N. Akther, S. Daer, S.W. Hasan, Effect of flow rate, draw solution concentration and temperature on the performance of TFC FO membrane, and the potential use of RO reject brine as a draw solution in FO–RO hybrid systems, Desalination Water Treat. 136 (2018) 65–71, https://doi.org/10.5004/dwt.2018.23195.
[22] S. Phuntsho, S. Hong, M. Elimelech, H.K. Shon, Osmotic equilibrium in the forward osmosis process: modelling, experiments and implications for process performance, J. Membr. Sci. 453 (2014) 240–252, https://doi.org/10.1016/j.memsci.2013.11.009.
[23] S.M. Ali, S.-J. Im, A. Jang, S. Phuntsho, H.K. Shon, Forward osmosis system design and optimization using a commercial cellulose triacetate hollow fibre membrane module for energy efficient desalination, Desalination 510 (2021) 115075, https://doi.org/10.1016/j.desal.2021.115075.
[24] A.M. Awad, R. Jalab, M.S. Nasser, M.K. Hassan, J. Minier-Matar, S. Adham, Pilot scale evaluation of thin film composite membranes for reducing wastewater volumes: osmotic concentration process, Emerg. Mater. 7 (2) (2024) 619–632, https://doi.org/10.1007/s42247-023-00495-y.
[25] R. Jalab, A.M. Awad, M.S. Nasser, I.A. Hussein, F. Almomani, J. Minier-Matar, S. Adham, Investigation of thin-film composite hollow Fiber forward osmosis membrane for osmotic concentration: a pilot-scale study, Korean J. Chem. Eng. 39 (1) (2022) 178–188, https://doi.org/10.1007/s11814-021-0935-9.
[26] Z. Wang, J. Zheng, J. Tang, X. Wang, Z. Wu, A pilot-scale forward osmosis membrane system for concentrating low-strength municipal wastewater: performance and implications, Sci. Rep. 6 (1) (2016) 21653, https://doi.org/10.1038/srep21653.
[27] V. Sanahuja-Embuena, G. Khensir, M. Yusuf, M.F. Andersen, X.T. Nguyen, K. Trzaskus, M. Pinelo, C. Helix-Nielsen, Role of operating conditions in a pilot scale investigation of hollow Fiber forward osmosis membrane modules, Membranes 9 (6) (2019) 66, https://doi.org/10.3390/membranes9060066.
[28] S.-J. Im, S. Jeong, A. Jang, Feasibility evaluation of element scale forward osmosis for direct connection with reverse osmosis, J. Membr. Sci. 549 (2018) 366–376, https://doi.org/10.1016/j.memsci.2017.12.027.
[29] M. Gulied, F. Al Momani, M. Khraisheh, R. Bhosale, A. AlNouss, Influence of draw solution type and properties on the performance of forward osmosis process: energy consumption and sustainable water reuse, Chemosphere 233 (2019) 234–244, https://doi.org/10.1016/j.chemosphere.2019.05.241.
[30] T. Majeed, S. Phuntsho, S. Sahebi, J.E. Kim, J.K. Yoon, K. Kim, H.K. Shon, Influence of the process parameters on hollow Fiber-forward osmosis membrane performances, Desalination Water Treat. 54 (4–5) (2015) 817–828, https://doi.org/10.1080/19443994.2014.916232.
[31] H.Y. Ng, W. Tang, W.S. Wong, Performance of forward (direct) osmosis process: membrane structure and transport phenomenon, Environ. Sci. Technol. 40 (7) (2006) 2408–2413, https://doi.org/10.1021/es0519177.
[32] Y. Xu, X. Peng, C.Y. Tang, Q.S. Fu, S. Nie, Effect of draw solution concentration and operating conditions on forward osmosis and pressure retarded osmosis performance in a spiral wound module, J. Membr. Sci. 348 (1–2) (2010) 298–309, https://doi.org/10.1016/j.memsci.2009.11.013.
[33] D.H. Jung, J. Lee, D.Y. Kim, Y.G. Lee, M. Park, S. Lee, D.R. Yang, J.H. Kim, Simulation of forward osmosis membrane process: effect of membrane orientation and flow direction of feed and draw solutions, Desalination 277 (1–3) (2011) 83–91, https://doi.org/10.1016/j.desal.2011.04.001.
[34] M.F. Gruber, U. Aslak, C. Hélix-Nielsen, Open-source CFD model for optimization of forward osmosis and reverse osmosis membrane modules, Sep. Purif. Technol. 158 (2016) 183–192, https://doi.org/10.1016/j.seppur.2015.12.017.
[35] W. Xue, K. Yamamoto, T. Tobino, C. Ratanatamskul, Modeling prediction of the process performance of seawater-driven forward osmosis for nutrients enrichment: implication for membrane module design and system operation, J. Membr. Sci. 515 (2016) 7–21, https://doi.org/10.1016/j.memsci.2016.05.037.
[36] D. Xiao, W. Li, S. Chou, R. Wang, C.Y. Tang, A modeling investigation on optimizing the design of forward osmosis hollow fiber modules, J. Membr. Sci. 392 (2012) 76–87, https://doi.org/10.1016/j.memsci.2011.12.006.
[37] A. Deshmukh, N.Y. Yip, S. Lin, M. Elimelech, Desalination by forward osmosis: identifying performance limiting parameters through module-scale modeling, J. Membr. Sci. 491 (2015) 159–167, https://doi.org/10.1016/j.memsci.2015.03.080.
[38] W.-J. Kim, O. Campanella, D.R. Heldman, A stepwise approach to predict the performance of forward osmosis operation: effect of temperature and flow direction, Desalination 538 (2022) 115889, https://doi.org/10.1016/j.desal.2022.115889.
[39] S.M. Ali, J.E. Kim, S. Phuntsho, A. Jang, J.Y. Choi, H.K. Shon, Forward osmosis system analysis for optimum design and operating conditions, Water Res. 145 (2018) 429–441, https://doi.org/10.1016/j.watres.2018.08.050.
[40] S. Hao, Z. Zhang, X. Zhao, X. An, Y. Hu, Investigation of multi-stage forward osmosis membrane process for concentrating high-osmotic acrylamide solution, Front. Membr. Sci. Technol. 3 (2024) 1407819, https://doi.org/10.3389/frmst.2024.1407819.
[41] F. Chen, L. Ma, Z. Zhang, X. Wang, Q. Wang, X. Wang, C. Chen, L. Jiang, X. Li, Pilot-scale evaluation of the sustainability of membrane desalination Systems for the Concentrate Volume Minimization of coal chemical wastewater, Environ. Sci.: Water Res. Technol. 10 (1) (2024) 205–215, https://doi.org/10.1039/D3EW00476G.
[42] S.-J. Im, N.D. Viet, B.-T. Lee, A. Jang, An efficient data-driven desalination approach for the element-scale forward osmosis (FO)-reverse osmosis (RO) hybrid systems, Environ. Res. 237 (2023) 116786, https://doi.org/10.1016/j.envres.2023.116786.
[43] J. Kim, G. Blandin, S. Phuntsho, A. Verliefde, P. Le-Clech, H. Shon, Practical considerations for operability of an 8″ spiral wound forward osmosis module: hydrodynamics, fouling behaviour and cleaning strategy, Desalination 404 (2017) 249–258, https://doi.org/10.1016/j.desal.2016.11.004.
[44] L. Sbardella, G. Blandin, A. Fàbregas, J. Carlos Real Real, A. Serra Clusellas, F. Ferrari, C. Bosch, X. Martinez-Lladó, Optimization of pilot scale forward osmosis process integrated with electrodialysis to concentrate landfill leachate, Chem. Eng. J. 434 (2022) 134448, https://doi.org/10.1016/j.cej.2021.134448.
[45] R. Jalab, A.M. Awad, M.S. Nasser, J. Minier-Matar, S. Adham, Pilot-scale investigation of flowrate and temperature influence on the performance of hollow Fiber forward osmosis membrane in osmotic concentration process, J. Environ. Chem. Eng. 8 (6) (2020) 104494, https://doi.org/10.1016/j.jece.2020.104494.
[46] J. Minier-Matar, M. Al-Maas, A. Hussain, M.S. Nasser, S. Adham, Pilot-scale evaluation of forward osmosis membranes for volume reduction of industrial wastewater, Desalination 531 (2022) 115689, https://doi.org/10.1016/j.desal.2022.115689.
[47] O.A. Bamaga, A. Yokochi, B. Zabara, A.S. Babaqi, Hybrid FO/RO desalination system: preliminary assessment of osmotic energy recovery and designs of new FO membrane module configurations, Desalination 268 (1–3) (2011) 163–169, https://doi.org/10.1016/j.desal.2010.10.013.
[48] B. Lian, G. Blandin, G. Leslie, P. Le-Clech, Impact of module Design in Forward Osmosis and Pressure Assisted Osmosis: An experimental and numerical study, Desalination 426 (2018) 108–117, https://doi.org/10.1016/j.desal.2017.10.047.
[49] J. Jeon, J. Jung, S. Lee, J.Y. Choi, S. Kim, A simple modeling approach for a forward osmosis system with a spiral wound module, Desalination 433 (2018) 120–131, https://doi.org/10.1016/j.desal.2018.01.004.
[50] S. Lee, Performance comparison of spiral-wound and plate-and-frame forward osmosis membrane module, Membranes 10 (11) (2020) 318, https://doi.org/10.3390/membranes10110318.

[51] Z.M. Binger, A. Achilli, Forward osmosis and pressure retarded osmosis process modeling for integration with seawater reverse osmosis desalination, Desalination 491 (2020) 114583.
[52] S. Mo, N. Sun, X. Liu, W. Zhu, T. He, Forward osmosis for concentrating Lithium-enriched brine: from membrane performance to system design, Desalination 591 (2024) 117997, https://doi.org/10.1016/j.desal.2024.117997.
[53] *Aquaporin Inside® HFFO®2*. Aquaporin. https://aquaporin.com/products/aquaporin-inside-hffo2/ (accessed 2025-02-04).
[54] R. Li, S. Braekevelt, J.L.N. De Carfort, S. Hussain, U.E. Bollmann, K. Bester, Laboratory and pilot evaluation of aquaporin-based forward osmosis membranes for rejection of micropollutants, Water Res. 194 (2021) 116924, https://doi.org/10.1016/j.watres.2021.116924.
[55] B. Kim, G. Gwak, S. Hong, Review on methodology for determining forward osmosis (FO) membrane characteristics: water permeability (a), solute permeability (B), and structural parameter (S), Desalination 422 (2017) 5–16, https://doi.org/10.1016/j.desal.2017.08.006.
[56] G. Blandin, A.R.D. Verliefde, C.Y. Tang, P. Le-Clech, Opportunities to reach economic sustainability in forward osmosis–reverse osmosis hybrids for seawater desalination, Desalination 363 (2015) 26–36, https://doi.org/10.1016/j.desal.2014.12.011.
[57] A. Achilli, T.Y. Cath, A.E. Childress, Selection of inorganic-based draw solutions for forward osmosis applications, J. Membr. Sci. 364 (1–2) (2010) 233–241, https://doi.org/10.1016/j.memsci.2010.08.010.
[58] A.H. Hawari, N. Kamal, A. Altaee, Combined influence of temperature and flow rate of feeds on the performance of forward osmosis, Desalination 398 (2016) 98–105, https://doi.org/10.1016/j.desal.2016.07.023.
[59] Y.C. Kim, S.-J. Park, Experimental study of a 4040 spiral-wound forward-osmosis membrane module, Environ. Sci. Technol. 45 (18) (2011) 7737–7745, https://doi.org/10.1021/es202175m.